Available online at www.sciencedirect.com

ScienceDirect

Journal of the European Ceramic Society 34 (2014) 1449–1455

www.elsevier.com/locate/jeurceramsoc

Short Communication

Bi-layer glass-ceramic sealant for solid oxide fuel cells

Allu Amarnath Reddy [a], Neda Eghtesadi [a], Dilshat U. Tulyaganov [b], Maria J. Pascual [c], Luis F. Santos [d], Surendran Rajesh [a], Fernando M.B. Marques [a], José M.F. Ferreira [a,*]

[a] *Department of Materials and Ceramic Engineering, CICECO, University of Aveiro, 3810-193 Aveiro, Portugal*
[b] *Turin Polytechnic University in Tashkent, 17, Niyazova Str., 100095 Tashkent, Uzbekistan*
[c] *Instituto de Cerámica y Vidrio (CSIC), C/ Kelsen 5, Campus de Cantoblanco, 28049 Madrid, Spain*
[d] *Department of Chemical Engineering/ICEMS, Instituto Superior Técnico/U Lisbon, 1049-001 Lisbon, Portugal*

Received 24 July 2013; received in revised form 31 October 2013; accepted 11 November 2013
Available online 5 December 2013

Abstract

A bi-layered concept of glass-ceramic (GC) sealant is proposed to overcome the challenges being faced by solid oxide fuel cells' (SOFCs). Two separated layers composed of glasses (Gd-0.3 and Sr-0.3) were prepared and deposited onto interconnect materials using a tape casting approach. After heat treating the bi-layered structure at 850 °C for 1–100 h, smooth and void free interfaces over the entire cross-section of joint were obtained. Micro-Raman analysis confirmed the presence of a higher amount of residual glassy phase in Gd-0.3 in comparison to Sr-0.3. The bi-layered GC showed good wetting and bonding ability to the Crofer22APU metallic plate. Slight increase of electrical conductivity with increasing annealing time was observed due to partial crystallization of the glass, but the overall conductivity levels of GC bi-layers were low enough to grant good electrical insulation. This set of relevant properties makes the investigated bi-layered sealants suitable for SOFC applications.

Keywords: Bi-layer; Glass-ceramic; Sealant; Interconnect

1. Introduction

During the past decades, continuous and significant worldwide efforts have been made for developing fuel cell materials/systems, especially solid oxide fuel cells (SOFCs).[1–4] However, some important challenges are still to be addressed towards fostering the commercialization of SOFCs. One of the major challenges respects to sealant materials, which are especially important for planar-SOFC for preventing fuel–oxidant mixing and providing electrical insulation of the stack layers under operation conditions. In particular, the metal–ceramic seals pose a significant challenge because of their severe functional requirements, encompassing the difficulties in selection the appropriate materials and associated processing optimization. Among the various materials proposed so far, glass and glass-ceramics (GC) exhibit superior properties.[5–7] To date, a number of rigid glasses and GCs sealants have been tested; in most cases, however, the stability of seals was insufficient due to: (i) coefficient of thermal expansion (CTE) mismatch; (ii) chemical interactions with SOFC components; and (iii) continuous devitrification behaviour.[8–13] Therefore, along with the design of new and more suitable glasses, additional new concepts/modifications are required to conquer the challenges being faced by the existing sealing technology.

Recently, we disclosed two different series of diopside-based glass systems thought for applications as sealants for SOFCs.[14–16] Among those, the systems designated as Gd-0.3 (in mol%: 20.62 MgO–18.05 CaO–7.74 SrO–46.40 SiO_2–1.29 Al_2O_3–2.04 B_2O_3–3.87 Gd_2O_3) and Sr-0.3 (in mol%: 24.54 MgO–14.73 CaO–7.36 SrO–0.55 BaO–47.73 SiO_2–1.23 Al_2O_3–1.23 La_2O_3–1.79 B_2O_3–0.84 NiO) presented superior properties (Table 1). Namely, both glasses revealed excellent thermal stability along a period of 1000 h and bonded well to the Sanergy HT metallic interconnect and 8 mol% yttrium stabilized zirconium (8YSZ) ceramic electrolyte without forming undesirable interfacial layers at the joints of SOFC components and GC. From Table 1 we can observe that both GCs exhibit similar properties, while differing in their amorphous fractions. Thus, using these glasses in the form of layer

* Corresponding author. Tel.: +351 234 370242; fax: +351 234 370204.
E-mail addresses: amarnathreddy@ua.pt (A.A. Reddy), jmf@ua.pt (J.M.F. Ferreira).

0955-2219/$ – see front matter © 2013 Elsevier Ltd. All rights reserved.
http://dx.doi.org/10.1016/j.jeurceramsoc.2013.11.012

Table 1
Properties of Gd-0.3 and Sr-0.3 glasses and glass-ceramics.[14–16]

	Gd-0.3	Sr-0.3
T_g (°C)	770	744
CTE × 10^{-6} K^{-1} (200–500 °C)	10.1 ± 0.1	11.2 ± 0.1
T_p (°C)	931	912
Sintering ability S_c (=$T_c - T_{MS}$)	52	29
T_D (°C)	875	869
Glass-ceramics produced after 1 h		
CTE × 10^{-6} K^{-1} (200–700 °C)	9.9 ± 0.1	11.2 ± 0.1
Shrinkage (%)	13.1	13.7
Mechanical strength (MPa)	96 ± 8	137 ± 7
Crystalline fraction (vol.%)	4	85
Glass-ceramics produced after 1000 h		
CTE × 10^{-6} K^{-1} (200–700 °C)	10.6 ± 0.1	10.4 ± 0.2
Shrinkage (%)	14.1	14.2
Mechanical strength (MPa)	134 ± 4	133 ± 5
Crystalline fraction (vol.%)	60	90

on layer, i.e. a bi-layer approach instead of a single layer between the metallic and ceramic plate of SOFCs might provide the following additional benefits: (i) a small gradient in the CTE that will lead to a lower thermal expansion mismatch between the sealing layers and the other SOFC components, thus providing enhanced mechanical reliability for the stack; (ii) cracks produced due to minor thermal stresses might be healed by the Gd-0.3 GC due to its sufficient amorphous content. In order to obtain good flow behaviour along with self-healing ability and appropriate viscosity (η), $\log \eta \approx 5$ at 850 °C (η in dPa s) is required.[17] GC compositions with crystalline/amorphous ratios of ~60/40 and with an ability to maintain stable crystalline phase assemblage during long runs have been considered suitable as a self-healing sealant for SOFC.[14,15] This communication presents the results and discusses the suitability of the Gd-0.3 and Sr-0.3 bi-layer approach for the application in SOFC stacks. The microstructural variations at the interface of the bi-layered GCs were assessed by micro-Raman spectroscopy.

2. Experimental

The chemical compositions of the experimental glasses, Gd-0.3 and Sr-0.3, and the detailed glass synthesis procedure were reported elsewhere.[14,15] Bi-layered compacts were prepared from 0.75 g of Gd-0.3 and 0.75 g of Sr-0.3 glass powders by depositing them in two uniform successive layers in a rectangular mould having dimensions of 4 mm × 5 mm × 50 mm and then uniaxial pressure (80 MPa) was applied to obtain rectangular bars. Cylindrical discs with 10 mm diameter were also prepared following the same procedure but using 0.3 g of each glass powder to study the interface between two layers and to determine the electrical conductivity of the bi-layers. The as obtained green bodies were sintered at 850 °C for 1 h and further heat treated for 100 h at a heating rate, $\beta = 5$ K min^{-1}.

Raman spectra were obtained using a Horiba LabRam HR 800 Evolution confocal Raman microscope, with a 532 nm excitation laser and a 100× objective lens (NA = 0.9). The incident laser power on the samples was ~10 mW and the spot size was ~3.14 square micron. The collected Raman radiation was dispersed with a 600 lines mm^{-1} grating and focussed on a Peltier-cooled charge-coupled device (CCD) detector allowing a spectral resolution of ca. 5 cm^{-1}. All spectra were recorded in the 100–4000 cm^{-1} range with an integration time of 1 s and 3 accumulations per spectrum.

The mechanical properties were evaluated by measuring the three-point bending strength (Shimadzu Autograph AG 25 TA, Columbia, MD; 0.5 mm min^{-1} displacement) using the rectangular bars. To investigate the adhesion of the bilayered glasses with the SOFC components, wetting experiments between the powdered glasses and interconnects (Crofer22APU and Crofer22H) were carried out. The separated layers were deposited using a tape casting approach. They were then superimposed and thermocompressed onto the interconnects. The diffusion couples were heated up to 850 °C at a relatively slow $\beta = 2$ K min^{-1} and kept at that temperature for 1 h and 100 h. Heat treatment was performed without applying any dead load. Microstructural observations were made by scanning electron microscopy (SEM; SU-70, Hitachi) with energy dispersive spectroscopy (EDS; Bruker Quantax, Germany) to study the distribution of elements along the GCs-interconnect diffusion couples and along the interface of GC layers.

The electrical conductivity (σ_e) of bi-layer GC was measured by AC impedance spectroscopy using a precision LCR metre (HP 4284A) in the frequency range of 20 Hz–1 MHz. The measurements were done on dense disc shaped samples within the temperature range of 650–800 °C in air, and under 10 vol.% H_2 + 90 vol.% N_2 atmosphere, using porous Pt electrodes and Pt current collectors.

3. Results and discussion

Figs. 1 and 2(a) and (b) show SEM cross-sections with different magnifications of the bi-layered GCs after sintering for 1 h and after further heat treating for 100 h at 850 °C, respectively. From the hot-stage microscopy tests performed for Sr-0.3 and Gd-0.3 compositions it was observed that heat treating the glass powder compacts at 850 °C was enough for obtaining fully dense GCs.[14,15] SEM micrographs revealed the smooth and voids free nature of the interfaces between the two glassy layers, indicating their good joining behaviour. This is further confirmed by the elemental mapping analysis for Gd, Sr and La elements, which enables differentiating the two glassy layers (Figs. 1d and 2d). Figs. 1c and 2c show the Raman spectra at the interfaces of the bi-layered GC structures sintered for 1 h (Fig. 1c) and further heat treated for 100 h (Fig. 2c). Micro-Raman allows getting complementary information by analysing different points at the interface within the micrometric range, not assessible by XRD. Both layers exhibit similar structural features (please see electronic supplementary information – ESI (Fig. ESI1)). However, the peaks are quite sharp in the case of Sr-0.3, whereas in Gd-0.3 they are much broader. This difference in peaks' definition can be understood based on the quantity of crystalline and glassy fractions present in the respective glasses. In general, broad Raman peaks are indicative of the glassy nature of materials. Thus, it is worth mentioning at this point that the high fraction

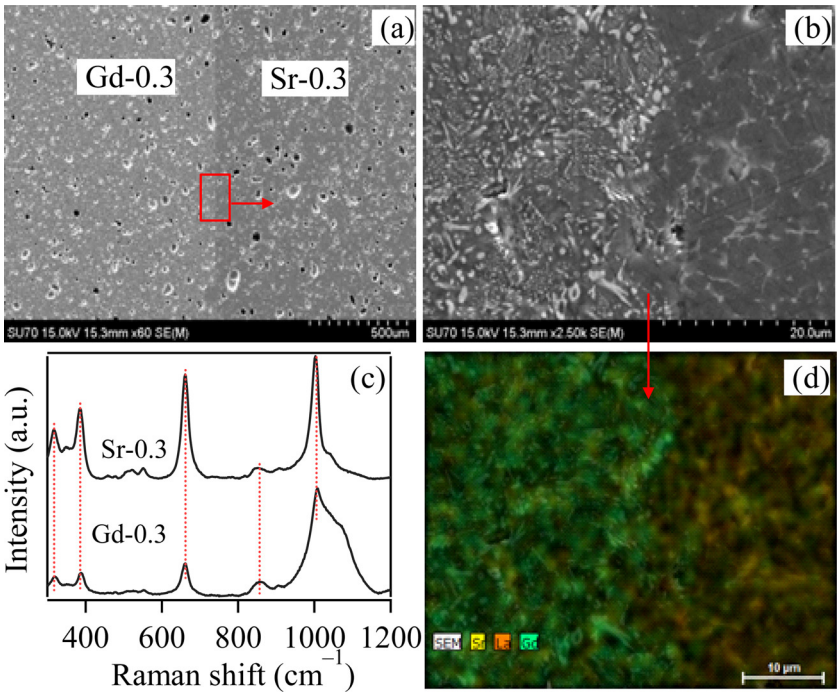

Fig. 1. Interface between Gd-0.3 and Sr-0.3 glass-ceramics after heat treating at 850 °C for 1 h: (a) and (b) SEM images; (c) Raman spectra; (d) elemental mapping.

of amorphous material presented in Gd-0.3 GC may be playing a crucial role in achieving the strong interaction and in the formation of the smooth interface between the two bi-layers. On the other hand, it is worthy mentioning that vibrational Raman bands observed for both Sr-0.3 and Gd-0.3 GCs were similar to those of synthetic diopside (Fig. ESI2) reported by Richet et al.[18] Micro-Raman analysis at the interface of bi-layered GC revealed that no further structural variations occurred during the further 100 h of heat treatment, except in intensity and full width half-maximum of the peaks. These changes were due to the partial conversion of glassy phase into crystalline phase (namely to the diopside[14,15]) along the heat treatment period. Micro-Raman mapping (Fig. ESI1) provides additional clearer information about this phase transition. These initial studies

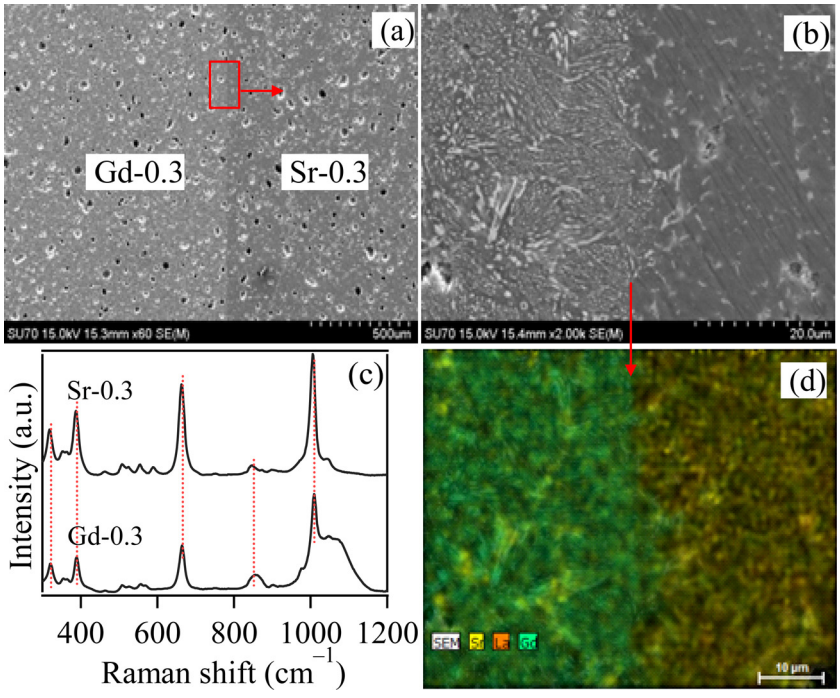

Fig. 2. Interface between Gd-0.3 and Sr-0.3 glass-ceramics after heat treating at 850 °C for 100 h: (a and b) SEM images; (c) Raman spectra; (d) elemental mapping.

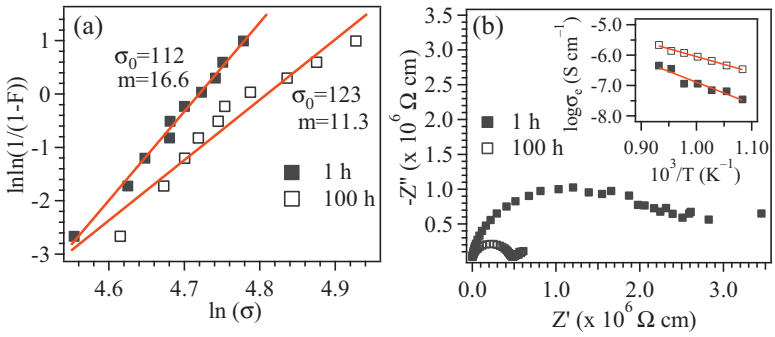

Fig. 3. (a) Weibull distributions of flexural strength values for the Gd-0.3/Sr-0.3 bi-layered glass-ceramics heat treated at 850 °C for 1 h, and (b) impedance spectra obtained at 800 °C in air of bi-layered glass-ceramics. The inset in (b) shows the temperature dependence of the electrical conductivity.

prove the suitability of the proposed glasses for the bi-layer approach, encouraging the application of this concept as sealant systems for SOFCs.

Mechanical strength values measured for the bi-layered GCs after sintering at 850 °C for 1 h, and after further heat treating for 100 h, were 105 ± 5 MPa and 118 ± 7 MPa, respectively. In order to characterize the quality of the bi-layer GCs, the two-parameter Weibull statistics was implemented based on the measured mechanical strength values. The obtained plots are presented in Fig. 3a. According to Weibull statistics, the increasing probability of failure (F) for a brittle material can be expressed by $F = 1 - \exp(-\sigma/\sigma_0)^m$, where F is the failure probability for an applied stress (σ), σ_0 is a normalizing parameter known as Weibull characteristic strength, and m is the Weibull modulus.[19] Here, the Weibull modulus m is a measure of the degree of strength data dispersion.[20] It can be observed that the failure probability function provides a reasonable fit to the experimental data. The obtained mechanical strength values for all the GCs being within the limits (22–150 MPa) required for SOFCs sealants make them suitable for this specific application.[21] The increase in mechanical strength of bi-layered GCs from 105 ± 5 MPa to 118 ± 7 MPa with increasing heat treatment time from 1 to 100 h is attributable to a greater extent of crystallization as can be deduced from the sharper Raman peaks after the longer thermal heat treatment. It is known that phase assemblage variations (types and volume fractions of crystalline/amorphous phases) in GCs upon isothermal treatments influence the mechanical strength of the seal. For example, a greater flexural strength was reported for the aged GC-9 glass sample in comparison to a non-aged one due to the increase of crystalline fraction.[22,23]

A potential problem in multi-/bi-layered materials is the crack growth between the contiguous layers. Cracks can derive from residual stresses generated at the interface due to large differences in the CTE and phase transitions. Thus, a close match of the CTEs of all components is essential for the mechanical integrity of the join between metal–ceramic or ceramic–ceramic components of SOFC. Apart from this, different shrinkage behaviours of the layers will also lead to delamination of the multi-/bi-layers. However, linear decreasing/increasing thermal expansion gradients with increasing number of layers will result in smaller residual stresses and, intuitively, one would expect that this would increase the crack growth energy in the layered materials.[24,25]

The CTE values of the glasses and GCs sintered at 850 °C for 1 h are presented in Table 1. Sr-0.3 exhibits the highest CTE ($11.2 \times 10^{-6}\,K^{-1}$) and shrinkage (13.7%) values. After the heat treatment period of 1000 h, both GCs exhibited the nearly equal CTE ($10.4 \times 10^{-6}\,K^{-1}$) and shrinkage (14.2%).[14,15] Considering these observations and the CTE values of metallic interconnects (Crofer22APU, Crofer22H) [(11–12) × $10^{-6}\,K^{-1}$] and of ceramic electrolytes (i.e. 8YSZ) [(10–12) × $10^{-6}\,K^{-1}$], the following bi-layer approach: ceramic electrolyte–Gd-0.3 glass–Sr-0.3 glass–interconnect, was adopted aiming at reducing the thermal stresses at the interfaces. Nevertheless, the stability of the bi-layered GC/interconnect couple might be deteriorated at further prolonged heat treatment due to the propensity of Gd-0.3 glass to continuous devitrification (Table 1).

Bi-layered GC seals bonded well to Crofer22H and Crofer22APU metallic interconnects since the investigated interfaces show homogeneous microstructures without any gaps being observed over their entire cross-sections of the joint. Figs. 4a, b and 5a, b show SEM images of the interfaces between bi-layered GCs and Crofer22H after 1 h and 100 h heat treatment at 850 °C, respectively. The corresponding EDS mapping for the relevant elements (Cr, Mn, Fe, and Si) existing at the Sr-0.3 GC/interconnect interface are also shown in Figs. 4 and 5. No diffusion layers were detected at the interfaces by SEM/EDS analyses within the limits of experimental uncertainty. Similar results were observed in the case of Croffer22APU after the samples heat treated for 1 h (Fig. ESI3).

Representative impedance spectra obtained in air at 800 °C for the bi-layered samples annealed at 850 °C either for 1 h or for 100 h, are shown in Fig. 3b. The spectrum of a sample sintered at 850 °C for 1 h shows a large and depressed arc covering almost the entire frequency range which suggests the contribution from different phases with distinct relaxation frequencies, maybe also some interfacial impedance between the seal layers, given their distinct composition and crystallinity. This is coherent with the analysis of the phase content of each layer, where both crystalline and glassy phases are present, and one of the layers is mostly amorphous (Table 1). At low frequency the spectrum is poorly defined, but a very small electrode tail can be assumed at such

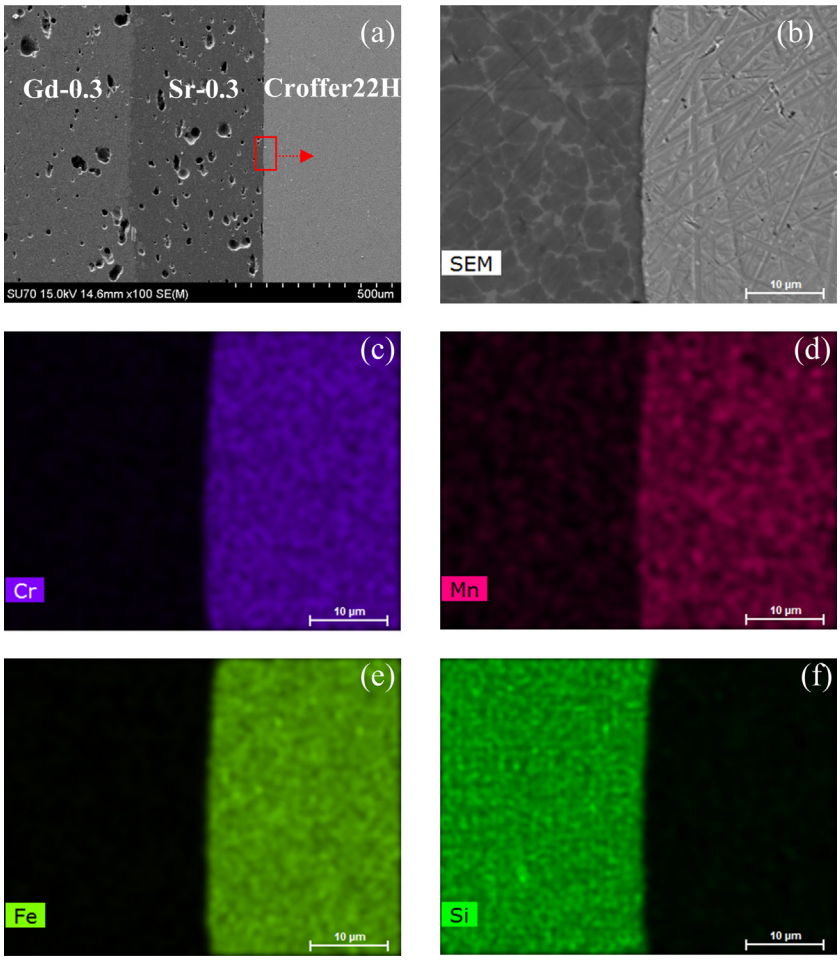

Fig. 4. SEM image and elemental mappings at the interfaces between Gd-0.3 GC/Sr-0.3 GC/Crofer22H after heat treatment at 850 °C for 1 h.

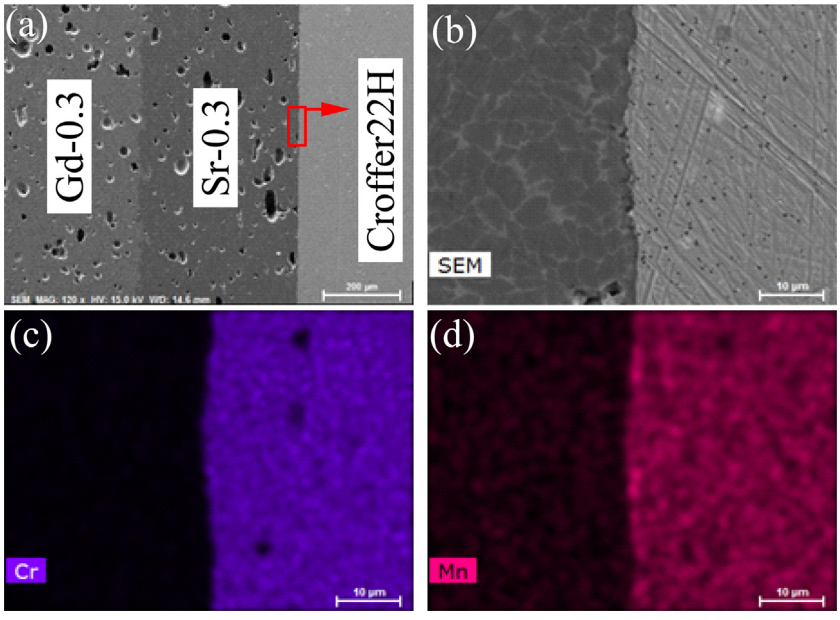

Fig. 5. SEM image and elemental mappings at the Interface between Gd-0.3 GC/Sr-0.3 GC/Crofer22H after heat treating at 850 °C for 100 h.

low frequencies. Considering the composition of these glasses, alkaline-earth ions are the most likely charge carriers.

In the case of samples sintered at 850 °C for 100 h the Nyquist plot obtained under the same conditions shows an almost regular semicircle which indicates the dominant contribution from a single phase. Considering the prolonged thermal treatment, the most likely explanation consists on the extensive crystallization of the glassy phases, providing a continuous ionic pathway throughout the entire bi-layer. If the glassy phases are still present, as suggested in Table 1, they are likely to provide only a parallel but least conductive pathway, since the conductivity of parallel arrangements is dominated by the most conductive element. This also means that this global conductivity is certainly a function of the thickness ratio of both layers, representing an average performance of the specific characteristics of this bi-layer assembly. The low frequency electrode tail is better defined in the case of samples annealed for 100 h, which indeed confirms the presence of dominant ionic conductivity in these samples. The possibility of a continuous ionic pathway throughout the entire bi-layer is a consequence of the layers composition, including common alkaline-earth cations.

The global bi-layer resistivity shows a considerable variation for samples annealed for 1 h or 100 h. For instance, at 800 °C the former sample has a resistivity 1.2 MΩ cm while the later has a resistivity of 0.2 MΩ cm. Irrespective of the already suggested dominant ionic transport through these bi-layer seals, the overall resistivity values are still high enough for the functional requirements of SOFC seals, enabling a good isolation between fuel cell components. As reference, in a SOFC, amongst electrolyte, cathode and anode, the least conductive cell component is the electrolyte with a target resistivity lower than 10 Ω cm at operating temperatures. In the worst case scenario (seal after 100 h), this means that the conductivity of the electrolyte is still four orders of magnitude higher than found for the seal. If we also consider the surface area/thickness ratios for currents crossing the electrolyte (high ratio) and sealant (extremely low ratio), we find an even more impressive relation between the cell output current and any internal parasitic current through the seal.

The temperature dependent electrical conductivity is shown in Fig. 3b inset. The activation energy calculated from the slope of the $\ln(\sigma_e T)$ versus $1/T$ plots is around 130 kJ mol^{-1} and 98 kJ mol^{-1} for samples annealed for 1 h and 100 h, respectively. The lower activation energies for the samples annealed for longer periods of time again suggest an easier ionic pathway through the bi-layer. This can be the result of enhanced crystallization in these samples (not only volume fraction but also average crystal/grain size), hypothesis coherent with the XRD results and involved process kinetics. Indeed, at constant temperature, interfaces and amorphous phases are expected to involve higher activation energies for ionic migration than crystalline phases.

4. Conclusions

1. Smooth and void free bi-layered GCs were successfully obtained. The high amount of glassy phase (96 vol.%) presented in Gd-0.3 glass enabled the formation of smooth interface and strong bonding with the Sr-0.3.
2. The as developed bi-layered GCs possess good mechanical reliability and wetting ability with Crofer22APU and Crofer22H, while having enough electrical resistivity.
3. Irrespective of the partial conversion of amorphous to crystalline phases with annealing at working temperatures, the global electrical conductivity of these GC bi-layers was at least four orders of magnitude lower than target values for the electrolyte layer. This low conductivity, presumably dominated by ionic transport, is clearly compatible with the electrical functional requirement imposed to efficient SOFC sealing materials.
4. Despite the interesting results achieved in this study, further experiments are needed for better evaluating the stability of the crystalline phase assembly of Gd-0.3 composition and its implications concerning the sealing performance at the SOFC's stack operation temperature.

Acknowledgements

This study was financially supported by the JECS trust (Contract 201242-2), University of Aveiro, CICECO, and FCT, Portugal (SFRH/BD/89915/2012 and PTDC/CTM-CER/114209/2009).

Appendix A. Supplementary data

Supplementary material related to this article can be found, in the online version, at http://dx.doi.org/10.1016/j.jeurceramsoc.2013.11.012.

References

[1]. Minh NQ, Takahashi T. *Science and technology of ceramic fuel cell*. Amsterdam, The Netherlands: Elsevier Science; 1995.
[2]. Shao Z, Haile SM. A high-performance cathode for the next generation of solid-oxide fuel cells. *Nature* 2004;**431**:170–3.
[3]. Choi JJ, Cho KS, Choi JH, Ryu J, Hahn BD, Yoon WH, et al. Low temperature preparation and characterization of LSGMC based IT-SOFC cell by aerosol deposition. *J Eur Ceram Soc* 2012;**32**:115–21.
[4]. Wachsman ED, Marlowe CA, Lee KT. Role of solid oxide fuel cells in a balanced energy strategy. *Energy Environ Sci* 2012;**5**:5498–509.
[5]. Fergus JW. Sealants for solid oxide fuel cells. *J Power Sources* 2005;**147**:46–57.
[6]. Mahapatra MK, Lu K. Glass-based seals for solid oxide fuel and electrolyzer cells – a review. *Mater Sci Eng Rep* 2010;**67**:65–85.
[7]. Mahapatra MK, Lu K. Seal glass for solid oxide fuel cells. *J Power Sources* 2010;**195**:7129–39.
[8]. Chou YS, Stevenson JW, Singh P. Novel refractory alkaline earth silicate sealing glasses for planar solid oxide fuel cells. *J Electrochem Soc* 2007;**154**:B644–51.
[9]. Zhang T, et al. Improving the chemical compatibility of sealing glass for solid oxide fuel cells: blocking the reactive species by controlled crystallization. *J Power Sources* 2012;**216**:1–4.
10. Zhang T, Brow RK, Fahrenholtz WG, Reis ST. Chromate formation at the interface between a solid oxide fuel cell sealing glass and interconnect alloy. *J Power Sources* 2012;**205**:301–6.
11. Gödeke D, Dahlmann U. Study on the crystallization behaviour and thermal stability of glass-ceramics used as solid oxide fuel cell-sealing materials. *J Power Sources* 2011;**196**:9046–50.

12. Stephens EV, Vetrano JS, Koeppel BJ, Chou Y, Sun X, Khaleel MA. Experimental characterization of glass-ceramic seal properties and their constitutive implementation in solid oxide fuel cell stack models. *J Power Sources* 2009;**193**:625–31.
13. Chang HT, Lin CK, Liu CK, Wu S-H. High-temperature mechanical properties of a solid oxide fuel cell glass sealant in sintered forms. *J Power Sources* 2011;**196**:3583–91.
14. Reddy AA, Tulyaganov DU, Pascual MJ, Kharton VV, Tsipis EV, Kolotygin VA, et al. Diopside–Ba disilicate glass-ceramic sealants for SOFCs: enhanced adhesion and thermal stability by Sr for Ca substitution. *Int J Hydrogen Energy* 2013;**38**:3073–86.
15. Goel A, Reddy AA, Pascual MJ, Gremillard L, Malchere A, Ferreira JMF. Sintering behavior of lanthanide-containing glass-ceramic sealants for solid oxide fuel cells. *J Mater Chem* 2012;**22**:10042–54.
[16]. Reddy AA, Tulyaganov DU, Pascual MJ, Kharton VV, Tsipis EV, Kolotygin VA, et al. SrO-containing diopside glass-ceramic sealants for solid oxide fuel cells: mechanical reliability and thermal shock resistance. *Fuel Cells* 2013, http://dx.doi.org/10.1002/fuce.201200237.
17. Pascual MJ, Guillet A, Durán A. Optimization of glass-ceramic sealant compositions in the system MgO–BaO–SiO_2 for solid oxide fuel cells (SOFC). *J Power Sources* 2007;**169**:40–6.
18. Richet P, Mysen BO, Ingrin J. High-temperature X-ray diffraction and Raman spectroscopy of diopside and pseudowollastonite. *Phys Chem Miner* 1998;**25**:401–14.
19. Weibull WA, Stockholm S. A statistical distribution function of wide applicability. *J Appl Mech* 1951;**18**:293–6.
20. Reddy AA, Goel A, Tulyaganov DU, Kapoor S, Pradeesh S, Pascual MJ, et al. Study of calcium–magnesium–aluminium–silicate (CMAS) glass and glass-ceramic sealant for solid oxide fuel cells. *J Power Sources* 2013;**231**:203–12.
21. Weil KS, Deibler JE, Hardy JS, Kim DS, Xia GG, Chick LA, et al. Rupture testing as a tool for developing planar solid oxide fuel cell seals. *J Mater Eng Perform* 2004;**13**:316–26.
22. Lin C-K, Lin K-L, Yeh J-H, Shiu W-H, Liu C-K, Lee R-Y. Aging effects on high-temperature creep properties of solid oxide fuel cell glass-ceramic sealant. *J Power Sources* 2013;**241**:12–9.
23. Chang HT, Lin CK, Liu CK. Effects of crystallization on the high-temperature mechanical properties of a glass sealant for solid oxide fuel cell. *J Power Sources* 2010;**195**:3159–65.
24. Sorensen BF, Sarraute S, Jorgensen O, Horsewell A. Thermally induced delamination of multilayers. *Acta Mater* 1998;**46**:2603–15.
25. Malzbendera J. Mechanical and thermal stresses in multilayered materials. *J Appl Phys* 2004;**95**:1780–2.